Visualization and Simulation of Bubble Growth in Pore Networks

X. Li and Y. C. Yortsos
Petroleum Engineering Program, Dept. of Chemical Engineering, University of Southern California, Los Angeles, CA 90089

Nucleation and growth of bubbles in porous media are important problems encountered in processes such as pressure depletion and boiling. Experiments and numerical simulations are studied in micromodel geometries to understand their basic aspects. Experiments of bubble growth by pressure depletion are carried out in 2-D etched-glass micromodels and in Hele-Shaw cells. Nucleation of bubbles and subsequent growth of gas clusters are visualized. Contrary to the bulk or Hele-Shaw cells, gas clusters in the micromodel have irregular and ramified shapes and share many of the features of an external invasion process (such as percolation during drainage). A pore network numerical model developed simulates the growth of multiple gas clusters under various conditions. It is based on the solution of the convection-diffusion equation and accounts for capillary and viscous forces, which play an important role in determining growth patterns. Numerical simulation agrees well with the experimental results.

Introduction

Bubble nucleation and bubble growth during pressure depletion in porous media are important problems encountered in processes such as solution-gas drive and boiling. The first is typical of oil recovery methods from underground reservoirs, when the reservoir pressure falls below the bubble point (Hunt and Berry, 1956). The second is common to enhanced boiling heat transfer (Thome, 1990), geothermal energy processes (Schubert and Strauss, 1977), and other applications (Doughty and Pruess, 1988). More generally, these problems involve important aspects of phase change in porous media. Here, the interaction between the pore microstructure and transport and capillary phenomena adds many novel aspects to the growth of the new phase, which are absent from the same processes in the bulk or from external displacements in porous media (Scriven, 1959; Plesset and Prosperetti, 1977; Lenormand et al., 1988). Bubble growth in porous media is still not fully understood and many theoretical and practical problems remain unresolved. In solution-gas drive processes, which are of main interest here, these include the value of the *critical gas saturation*, S_{gc}, denoting the minimum gas volumetric content before the onset of bulk gas flow and the effect of pressure decline rate on growth (De Swaan, 1981; Firoozabadi et al., 1989; Li and Yortsos, 1993). Their consideration is important for the optimal design of various oil recovery methods, particularly in fractured systems, where the solid matrix has low permeability (Kamath and Boyer, 1993). Analogous problems exist in boiling. In either application, the state of the art is mostly phenomenological, and it is typically based on the use of various forms of effective medium approximations.

This article focuses on the growth of a single-component gas from a saturated two-component liquid, driven by a decline in the liquid pressure. Related work on the boiling problem is in progress (Satik, 1994). Previous research on these problems has been incomplete (Hunt and Berry, 1956; Moulu and Longeron, 1989; Kortekaas and Poelgeest, 1989). Early attempts focused mostly on nucleation characteristics (Hunt and Berry, 1956; Moulu and Longeron, 1989), with only limited attention paid to the subsequent growth. Particularly interesting is the effect of pressure decline rate. Some authors have used expressions from homogeneous nucleation to surmise effects of pressure decline on the overall growth process (Moulu and Longeron, 1989). Others have applied concepts from bubble growth in the bulk, using compact, noninteracting bubbles to describe gas-phase growth (Kashchiev and Firoozabadi, 1993a,b). Experimental support for porous media processes has been limited. Most experiments in laboratory cores are typically interpreted based on an integrated response of the

Correspondence concerning this article should be addressed to Y. C. Yortsos.

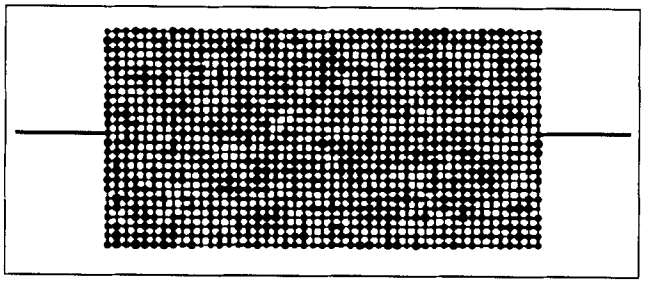

Figure 1. Pore network and glass micromodel pattern.

system rather than *in situ* observations. This approach is inherently inadequate to resolve important small-scale issues.

A previous study (Yortsos and Parlar, 1989) provided the first model that emphasized the effect of pore structure in controlling the growth patterns and postulated the existence of percolation-like gas clusters. We proceeded by separating nucleation from bubble growth. From an analysis of the nucleation problem, we postulated that the occupancy of a pore, which for all practical purposes signals the onset of observable nucleation, is controlled by capillary heterogeneities in the pore surface (such as cavities) that trap gas microbubbles. We then proceeded to relate the onset of nucleation to the condition that the local supersaturation exceeds their capillary barrier. For example, assuming a nucleation site (cavity) of half-width W, the critical supersaturation for its activation would be $\Delta P \equiv KC - P_l \sim 2\gamma/W$, where K is the solubility constant, C and P_l denote local concentration and liquid pressure, respectively, and γ is the interfacial tension. According to this model, therefore, the effect of the pressure decline rate would be in activating such sites rather than in modifying the kinetics of homogeneous nucleation, as previously has been postulated. Similar conclusions on the role of surface heterogeneities were reached in a more recent experimental study by Yousfi et al. (1991).

Yortsos and Parlar (1989) also formulated the equations for bubble growth in porous media and proceeded with a qualitative delineation of the various patterns. However, they were able to obtain quantitative results only in the limiting case of very low supersaturations, where concentration gradients are weak and the process is controlled only by capillary forces. A condition on the pressure decline rate was derived for this regime to be applicable. Under this condition, the problem can be approached as invasion percolation from multiple internal growth sites. The analysis shows that the gas saturation (pore volume fraction) is then only a function of pressure and of the fraction of activated sites. The importance of capillarity and the possible emergence of a percolation regime were qualitatively verified in preliminary experiments by Yousfi et al. (1990), who studied the liberation of CO_2 gas from supersaturated carbonated water in micromodels. Their results confirmed the existence of specific nucleation sites and the subsequent growth of gas bubbles in the form of ramified clusters. Visualization studies of solution gas drive at high pressure and temperature were also conducted by Danesh et al. (1987) with the use of organic compounds. These authors focused on the onset of nucleation, which also occurred in specific sites (which happened to coincide with the largest pore body), and on certain local mechanisms of growth.

While these studies offered much insight in the micromechanics of the process, a host of questions still remain unanswered. For example, the simple theory of Yortsos and Parlar (1989) does not address effects of pressure decline rate on bubble growth, the type and growth rates of the various patterns, or the competition between growing clusters. In the analogous problem of phase growth in the bulk, competition between growing compact (spherical) particles is usually subject to Ostwald ripening (Lifshitz and Slyozov, 1961), the larger sizes growing at the expense of the smaller ones. A different mechanism is expected in porous media, where due to the microstructure, the local gas-liquid curvature is unrelated to the cluster size. Of much interest also are process scale-up and finite size effects.

In a recent investigation, described in the companion publications (Li and Yortsos, 1994, 1995; Satik et al., 1995), we have revisited the problem of bubble growth in porous media. Li and Yortsos (1994) considered bubble stability in an *effective* porous medium, where a new stabilizing mechanism on the growth of the new phase was identified. That study has relevance to the delineation of growth patterns in effective media, such as a Hele-Shaw cell, where the local microstructure is absent. The effect of microstructure was emphasized in Satik et al. (1995) and Li and Yortsos (1995). Scaling laws for the growth of a single cluster were proposed in Satik et al. (1995), while a general theory for growth of multiple clusters was formulated in Li and Yortsos (1995). These two theoretical studies rely on experimental observations and numerical simulations described in this article. Here, we report on visualization experiments, conducted in etched glass micromodels, as described in Yousfi et al. (1990), and in Hele-Shaw cells. The growth of a gas phase from a supersaturated carbonated water solution, driven by a pressure decline, is studied. In particular, we focus on nucleation aspects and on the mode of pore occupancy. Subsequently, a pore network is developed to describe gas-phase growth. The experiments are simulated with the use of the pore network model.

Experiments

To obtain an insight on the micromechanics of bubble growth, visualization experiments were conducted. Following Yousfi et al. (1990), we considered the liberation of CO_2 gas from saturated carbonated water contained in an etched-glass micromodel. The micromodel was prepared by etching a 2-D square network pattern of pores and throats on a glass plate (Figure 1), which was subsequently fused to another glass plate to create a 2-D pore network. Details of the fabrication process can be found in Chatzis (1982). Pore-throat and pore-body-size distributions were selected from the Rayleigh distribution shown in Figure 2. Due to imperfections in the glass and the lack of precise control in etching and fusion, however, the final pattern is not identical to the original. As will be shown below, this places limitations on the ability to exactly reproduce the experimental results by numerical simulation. For comparison purposes, experiments were also conducted in a Hele-Shaw cell, which was constructed from two parallel glass plates of dimensions 2.5×10 cm separated by a spacing of 200 μm.

The experimental setup is shown in Figure 3. A helium gas tank and a flow controller were used to control the pressure decline rate. The experimental procedure was as follows:

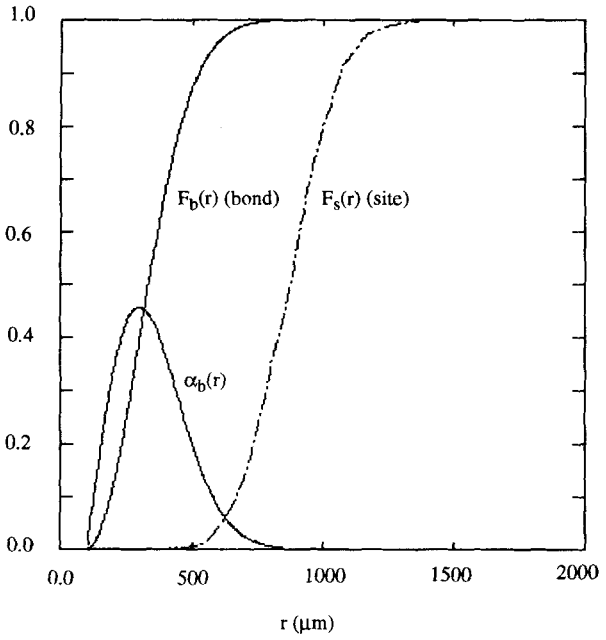

Figure 2. Rayleigh distributions of pore throat (bond) and pore body (site) sizes.

(1) CO_2 gas was first injected to displace air from the glass micromodel or the Hele-Shaw cell.

(2) Subsequently, distilled water was injected at a high pressure, typically around 60 psi (413 kPa) to saturate the micromodel.

(3) Supersaturated carbonated water was injected along with a coloring dye to displace the distilled water. We typically used a saturation pressure of about 56 psi (386 kPa).

(4) The micromodel was connected to the helium gas tank and the system pressure was reduced at the specified decline rate by releasing helium gas.

(5) The process was videotaped and the system pressure was recorded.

Shown in Figure 4 is a typical sequence of bubble growth in the glass micromodel for a pressure decline rate of 8.64 psi/h (59.5 kPa/h). The onset of growth occurs from various nucleation sites, which become activated at different stages of the process, usually after a certain supersaturation level was reached. A wide range of supersaturations for different systems has been reported in the literature (Kamath and Boyer, 1993; Kennedy and Olson, 1952; Stewart et al., 1954; Wieland and Kennedy, 1957). In our glass micromodel experiments, we observed supersaturations varying from 5 to 30 psi (35 to 207 kPa). This is consistent with cavity sizes W of the order of 1-10 μm. Occasionally, we were able to observe an activation event. The sequence of Figure 5 shows the detachment from the surface and the subsequent growth of a microbubble, orig-

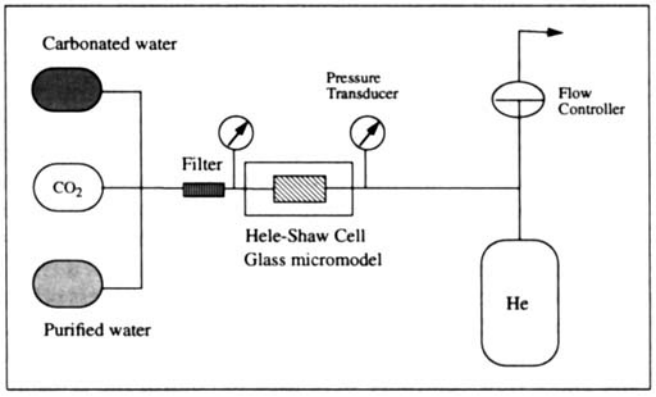

Figure 3. Experimental apparatus.

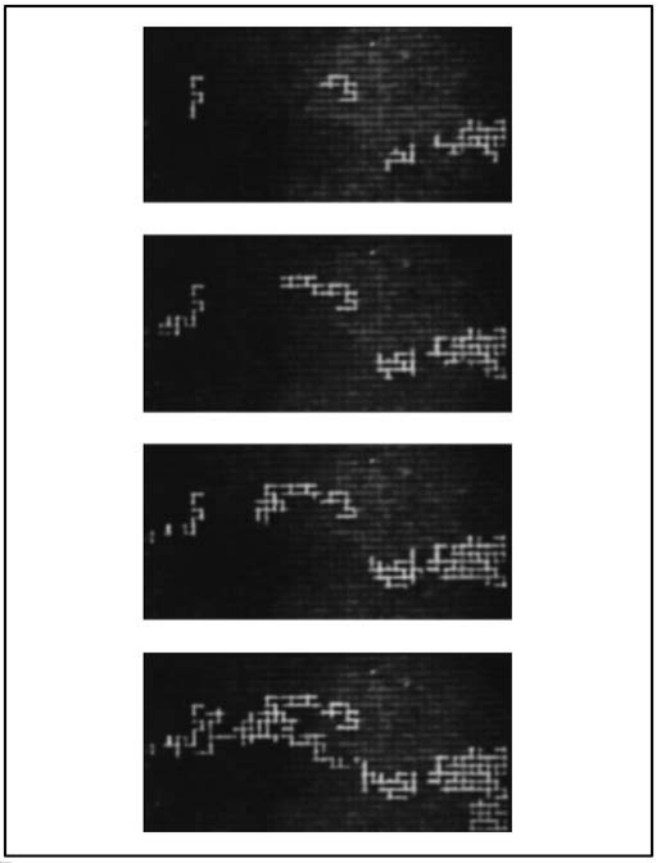

Figure 4. Growth patterns in the glass micromodel for $a = 8.64$ psi/h (59.5 kPa/h).

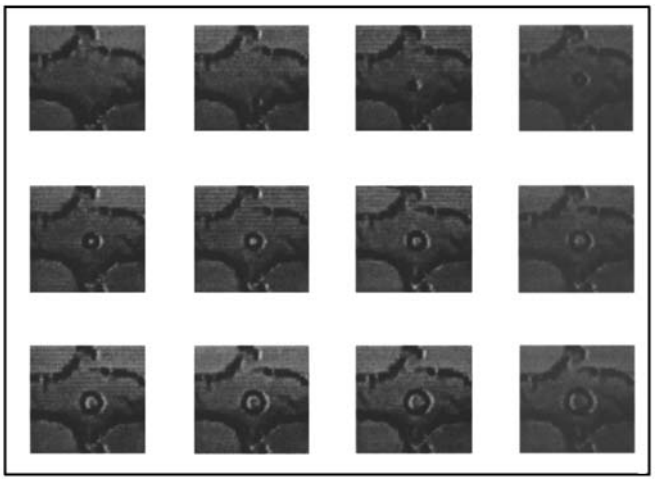

Figure 5. Site activation event (12 snapshots at 1-s intervals).

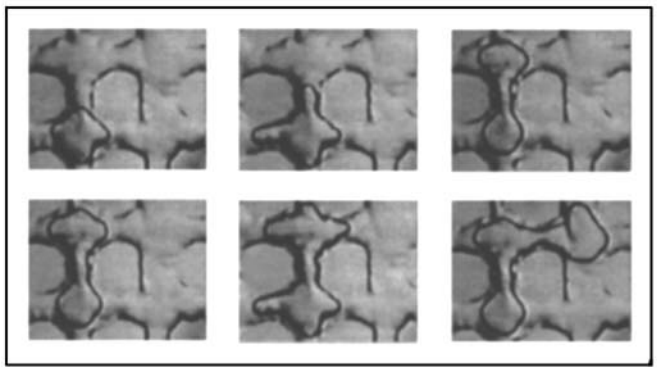

Figure 6. Porescale sequence of gas bubble growth.

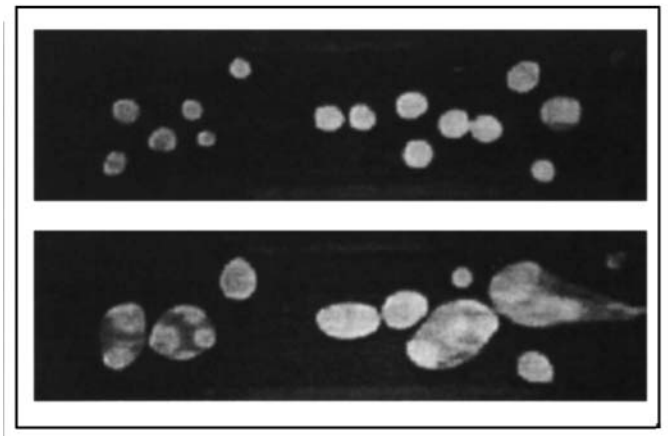

Figure 7. Bubble growth in a Hele-Shaw cell.

inally trapped at pore surface heterogeneities. The time elapsed from the macroscopic appearance of the microbubble (first frame) to its detachment, growth, and subsequent occupancy of the pore body (last frame) is of the order of a few seconds, suggesting that for practical purposes one can identify the condition for the occupancy of a pore body with that for the release of the trapped microbubble from a surface cavity. Although of heterogeneous origin, however, nucleation was not reproducible. We suspected that this was due to the injected dye particles, which often acted as nucleation sites. The frequency of nucleation decreased substantially when the experiments were carried out in the absence of dye. The lack of reproducibility of nucleation affects significantly the trends observed, as discussed below.

Subsequent to nucleation, gas clusters begin to grow in an irregular, often ramified, fashion (Figure 4). Trapping of the displaced liquid phase, which is characteristic of invasion percolation processes in external displacement, was frequently observed. A typical sequence of the growth of a gas cluster shown in Figure 6 involves two steps: (i) A slow pressurization step, during which the pressure in the cluster increases and the gas-liquid menisci move only slightly to adjust their curvature to the pore geometry; and (ii) A fast penetration step (similar to "rheon" events in drainage, Payatakes and Dias, 1984) immediately after a capillary barrier at a perimeter throat is exceeded. In all our experiments, which involve pressure decline rates in the range 0.1–60 psi/h (0.7–413 kPa/h), cluster growth occurred by penetration of only one perimeter throat per cluster at a time. Following this step, the volume of the cluster increased, as the new invaded site became occupied, while further slight adjustment of all interfaces was noted. This sequence was repeated in the next event. By contrast, in experiments involving Hele-Shaw cells, although also initiated from different nucleation sites, the gas clusters grow in a compact almost perfectly radial fashion following a macroscopically smooth movement (Figure 7). Bubble coalescence eventually produces large nonradial clusters, however, the patterns remain compact at all times. The difference between the two growth patterns is due to the microstructure of the glass micromodel. A similar difference is also seen in typical external displacements (such as comparison of viscous fingering patterns in Hele-Shaw cells and in porous media, Homsy (1987), and can be analyzed using statistical physics theories, such as percolation and DLA (diffusion-limited aggregation) (see Satik et al. (1995) and Li and Yortsos (1995) for an application in the present context).

Typical pressure-gas saturation (pore volume fraction) curves at two different pressure decline rates in a 44×24 micromodel are shown in Figure 8. Gas saturation denotes the volume fraction of the pore space occupied by the gas. It is shown that as the decline rate increases, the gas saturation corresponding to a given pressure decreases. This is consistent with analogous experiments in laboratory cores (Kortekaas and Poelgeest, 1989), as well as with the numerical simulations to be shown below. The critical gas saturation, corresponding to the onset of gas flow in the production outlet, was found to be slightly higher in the experiment involving a lower pressure decline rate. This trend is opposite to recent experimental results (Kortekaas and Poelgeest, 1989; Firoozabadi et al., 1989; Kashchiev and Firoozabadi, 1993b), although it must also be noted that Kamath and Boyer (1993) observed no significant effect of the pressure decline rate in their low rate experiments. This discrepancy is due to the following: For an unambiguous definition, a critical gas saturation should be identified with the value at which a sample-spanning cluster forms (in a manner similar to a percolation cluster, although here growth also occurs from multiple sites and mass transfer is an additional factor, Satik et al. (1995); Li and Yortsos (1995). Based on this definition, the theory developed by Li and Yortsos (1995) shows that, provided that the nucleation sites are permanently

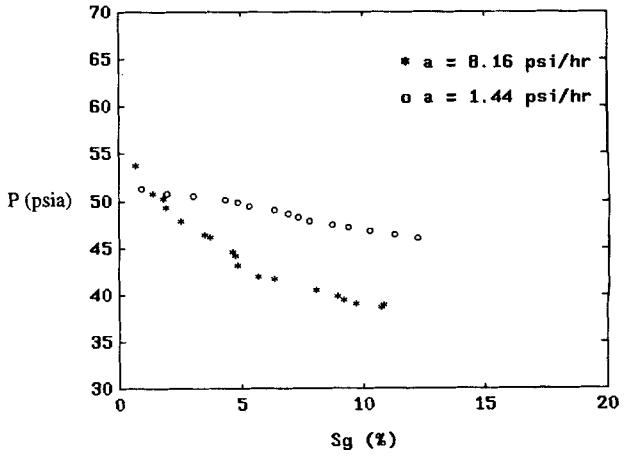

Figure 8. Experimental pressure-saturation curves for two different pressure decline rates.

fixed and that nucleation is *reproducible*, higher pressure decline rates lead indeed to higher critical gas saturations, because of an increase in the number of activated sites. In laboratory experiments, the critical point is usually identified when gas starts flowing at the outlet of the porous medium. If care is not taken to also ensure that this signals the formation of a sample-spinning cluster, this value would be subject to nontrivial finite-size effects, as it would be significantly affected by the random occurrence of some nucleation sites near the production outlet. (In fact, in such cases, the error in the estimation of S_{gc} would increase with its true value.) This was the case in our experiments, where the process terminated at the time gas starts flowing out of the production outlet, even though a sample-spanning cluster was not reached (Figure 4). In addition, in our experiments, nucleation events were *not* reproducible, due to the presence of the coloring dye particles, which frequently acted as nucleation sites. It is our experience that if nucleation is not reproducible, namely if nucleation sites and their activation threshold are not fixed, the value of critical gas saturation would actually be a random variable, the sensitivity of which to the pressure decline rate would accordingly be subject to uncertainty.

Pore Network Simulation

To simulate the experiments and to provide a working model for the process, we proceeded with a pore network simulation. A detailed simulation of the full problem, perhaps with the use of lattice gas simulation (Rothman, 1988), is not the main scope of this investigation. We will take the simpler, but less accurate, approach of pore network simulation.

Pore network simulators are useful tools for understanding displacements in porous media and have been frequently used in past investigations (Lenormand et al., 1988; Blunt and King, 1991), particularly in immiscible displacement. In such models, the porous medium is represented by an equivalent network of pores of distributed sizes, joined by bonds of another size distribution. Pores are taken to represent the storage capacity of the porous medium, and bonds represent flow resistance and provide capillary pressure thresholds. Interfaces are allowed to reside only in pore bodies, the occupancy of which is partial, in general, and dictates the volumetric content of the site. Capillary effects within a pore body are generally not considered. After complete occupancy of the pore body, the meniscus can invade a neighboring pore throat if the corresponding capillary barrier is exceeded. Consistent with these rules, we developed a pore network simulator, where both flow and concentration fields were computed. For a computationally manageable simulation, it was necessary to make certain approximations, such as neglecting the snap-off of gas-liquid interfaces that may occur when certain bonds are penetrated (although such events are rare before the onset of bulk gas flow). The following rules were used:

(1) The network consists of pores and bonds. The pores provide volumetric storage, and the bonds control fluid pressure drops and capillary characteristics. A Rayleigh distribution shown in Figure 2 was used to randomly assign pore sizes.

(2) Pore bodies can be filled by the gas phase, the liquid phase or both. Pores occupied by liquid can become trapped by gas-occupied pore bodies, if topologically possible. When a pore is trapped, liquid-phase movement is not allowed, although diffusion continues.

(3) The capillary pressure within a pore body is neglected. The capillary pressure across an interface at the entrance of a bond is inversely proportional to the bond radius.

(4) The gas phase is isothermal and inviscid and the gas-phase pressure is spatially uniform for all pores belonging to the same cluster, although the gas-phase pressure may be different in different gas clusters.

(5) Bond penetration takes place when a pore is fully occupied by gas and the difference between gas- and liquid-phase pressure exceeds the capillary pressure at the entrance of a bond. There is no limitation on the number of bonds that can be penetrated at each time step.

We consider bubble growth in a pore network, such as the micromodel of Figure 1, the lateral boundaries of which are closed to flow, with the exception of two producing sites at opposite ends. Initially, the medium is occupied by a supersaturated liquid, the pressure of which at the producing side (or in the far field). $P_{l\infty}$, subsequently declines either at a specified rate $a \equiv -dP_{l\infty}/dt$, or by an abrupt lowering of its value. Constant pressure decline rates are common to many practical applications. To model the nucleation stage, we must specify both the location and the supersaturation level for the activation of nucleation sites. In the simulations of the experiments described below, these were determined by direct observation. If a simple cavity model is used (for a detailed discussion, see Atchley and Prosperetti, 1989), the activation of a site requires:

$$KC - P_l \geq \frac{2\gamma}{W} \tag{1}$$

where we assumed for simplicity, but without loss in generality, the linear solubility condition:

$$P_g = KC \tag{2}$$

between the gas pressure, P_g, and the concentration, C, of the volatile component (dissolved gas) at the gas-liquid interface. More generally, one can dispense with a particular model by simply assigning a distribution of nucleation sites at various locations with a distribution of local supersaturations.

Following nucleation, individual gas clusters grow by mass transfer of solute in the liquid-occupied pore space. In a continuum model, mass transfer is described by the usual convection-diffusion equation:

$$\frac{\partial C}{\partial t} + \boldsymbol{u} \cdot \nabla C = D \nabla^2 C \tag{3}$$

where D is the molecular diffusivity, while at creeping flow conditions and in the absence of gravity, the liquid velocity $\boldsymbol{u}$ obeys Stokes' law:

$$\nabla P_l = \mu \nabla^2 \boldsymbol{u} \tag{4}$$

In the simulations, however, discrete forms of these equations were used. For example, the mass balance for the nonvolatile component was expressed as:

$$\sum_j Q_{ij} = 0 \tag{5}$$

for site i, where Q_{ij} refers to volume flow rate between adjacent sites i and j. The sum is over all neighboring sites j, and we used Poiseuille's law to solve the Stokes Eq. 4:

$$Q_{ij} = \frac{A_{ij} r_{ij}^2 \Delta P_{ij}}{8\mu l_{ij}} \tag{6}$$

where A_{ij} is the cross-sectional area of the pore throat joining sites i and j, r_{ij} is the corresponding distributed throat radius, and l_{ij} is the bond length. The mass balance for solute in site i reads:

$$(1.0 - S_{gi}) V_s \frac{\Delta C_i}{\Delta t} = \sum_j \left[D A_{ij} \frac{\Delta C_{ij}}{l_{ij}} \right] + \sum_j \left[\frac{A_{ij} r_{ij}^2 \Delta P_{ij}}{8\mu l_{ij}} C_{ij} \right] \tag{7}$$

where V_s is the site volume, and S_{gi} is its gas volumetric content ($S_{gi} \neq 0$ if the site happens to belong to the cluster). Equation 7 can be viewed as the finite-difference analog of the mass balance (Eq. 3). We must point out that despite the fact that pressure gradients and flow velocities are typically quite small, their consideration is necessary in order to account for convection. This has corresponding implications on the complexity of the numerical algorithm. The gas phase is taken isothermal and inviscid, such that the pressure within a connected gas cluster is spatially uniform. Different gas clusters may have different pressures, however. We use the ideal gas law:

$$P_{gk} V_k = n_k R T \tag{8}$$

to relate pressure, P_{gk}, volume, V_k, and mole content, n_k, of a cluster of size k. From the visualization experiments, we have observed that cluster growth occurs in two steps: A pressurizing step and a penetrating (pore filling) step. We approximate the pressurizing step with a process of constant V_k and increasing P_{gk}, and the penetration step with a process of constant P_{gk} and increasing V_k. The latter takes place when capillary equilibrium at any gas-liquid interface at the cluster perimeter becomes unstable.

The above equations are subject to the appropriate flux or concentration conditions at the boundaries, and to the condition that the concentration on the interface of each cluster is spatially constant. In the numerical simulation, finite increments in time, concentration, and pressure were used. The set of equations were solved by an SOR (successive overrelaxation) method. The computational algorithm is explained in detail in Li (1993) and involves the following:

(*1*) *Nucleation.* Nucleation sites and their supersaturations were distributed at random (or as specified from experimental observations). The host pore body is assumed to become fully occupied by gas immediately after the activation of the nucleation site.

(*2*) *Pressurization Step.* When all pores in the gas cluster are fully occupied, mass transfer from the liquid to the gas leads to a gas pressure increase, and a throat is eventually invaded. During this step, there is no liquid flow, and the concentration field is determined in the absence of convection. When the smallest capillary pressure threshold at the perimeter is reached, the corresponding bond is penetrated. The capillary threshold is conventionally described by:

$$P_{gk} - P_l = \frac{2\gamma}{r_{ij}} \tag{9}$$

where $2\gamma/r_{ij}$ is the local capillary pressure. The time required to complete this process is determined by a trial-and-error procedure.

(*3*) *Penetration (Pore-Filling) Step.* When partially occupied pores exist in the perimeter of the gas cluster, mass diffusion and (possible) pressure decline eventually lead to their full occupancy. The filling of these pores is carried out in discrete time steps, during which only one of the partially occupied pores becomes fully occupied. We should note that the meniscus displacement is subject to the usual kinematic and mass-transfer conditions:

$$v_n = \frac{u_n}{1 - \frac{\rho_g}{\rho_l}} \sim u_n \tag{10}$$

and

$$\rho_g (v_n - u_{gn}) = D \frac{\partial C}{\partial n} \tag{11}$$

where v_n, u_n, and u_{gn} are the normal components of the interface velocity, the liquid velocity, and the gas velocity at the interface, respectively. In general, the determination of u_{gn} requires that the momentum balance in the gas phase be also considered. This was not done here (but see Li and Yortsos, 1994). Instead, we proceeded by solving only for the integral balance (Eq. 8) over each cluster. The following trial-and-error rules were used:

(a) First, an initial guess for the gas pressure P_{gk} is assumed for each gas cluster, based on which the momentum balance (Eq. 5) was solved and the liquid pressure field was, therefore, determined.

(b) Based on the pressure field, the flow rate Q_i at each partially-gas-occupied site i is determined, from which the shortest time to fully occupy one of these sites is found:

$$\Delta t_{\min} = \min \left(\frac{V_j}{Q_j} \right) \tag{12}$$

where V_j is the liquid volume displaced from pore j. The volume displaced from each site in the time $\Delta t_{\min}$ is then recalculated to yield the overall volume change in the cluster during this step:

$$\Delta V_k^{(f)} = \Delta t_{\min} \sum_j Q_j \tag{13}$$

where the summation is over all partly occupied perimeter sites.

(c) The corresponding net mass transfer, m_k, into cluster k is next calculated by solving the mass balance Eq. 7 with the appropriate boundary conditions. The volume change of the gas cluster due to mass transfer is then:

$$\Delta V_k^{(m)} = \frac{m_k RT}{M_w P_{gk}} - \frac{V_k \Delta P}{P_{gk}} \tag{14}$$

This equation represents the ideal gas law (Eq. 8) expressed in finite-difference forms. Based on the difference between $\Delta V_k^{(f)}$ and $\Delta V_k^{(m)}$ additional iterations are taken on the assumed gas pressure P_{gk} until convergence is reached. Finally, at the end of each time step, a check is made to determine if any new nucleation sites are activated and to determine whether conditions exist for additional perimeter throats to be penetrated.

Simulation of Experimental Results

To test the validity of the simulator, the glass micromodel experiments were simulated. The geometry of the network used in the simulation is the same as the computer pattern used to construct the glass micromodel. However, the true sizes of the micromodel pores are likely to be somewhat different due to various defects during the fabrication process, as explained above. For each experiment simulated, information from the actually observed nucleation events (location and time) was used as input to the numerical model. Because of the 2-D nature of the micromodel, the pores and throats were approximated as equivalent circular plates and rectangular channels. Even though the etching depth of the glass micromodel is unknown, it does not significantly affect the simulation results, because it affects site volumes and mass-transfer areas in equal proportions. For calculation purposes, a value of 500 μm was used in all simulations.

The following values were assigned to the physical variables: $\mu = 1$ cp, $\gamma = 72$ dyne/cm, $T = 530$ R, and $M_w = 44$. The solubility parameters were estimated from the data reported by Quinn and Jones (1936).The gas solubility constant K was calculated to be 8,820 psi (61 MPa)/(g/cm^3). All experiments were carried out at the initial pressure of 71.4 psia (492 kPa) corresponding to an initial concentration of 0.0081 g/cm^3. Diffusion coefficients of CO_2 in water were reported in the range 1.0×10^{-5} to 3.0×10^{-5} cm^2/s (Vivian and King, 1964). The effect of the diffusivity on the process is quite important. Shown in Figure 9a is a plot of the simulation of an experiment at the low-pressure decline rate of 1.44 psi/h (9.92 kPa/h), during which ten nucleation sites were activated. Since a diffusivity value was not actually measured, we selected the value of 3.0×10^{-5} cm^2/s, which best fitted this experiment. The value is consistent with the published data. The corresponding simulated cluster pattern is shown in Figure 9b. Such patterns are typical of the growth patterns generated by the numerical algorithm. Based on the above parameter values and on the original network pattern, we tested the simulator for various experiments conducted in two different glass micromodels of sizes 44×24 and 65×35, respectively. Several runs at different pressure decline rates with varying nucleation fractions were conducted and simulated. Additional details can be found in Li (1993).

Experimental and simulated results of pressure-saturation (pore volume fraction) curves, which represent the overall system behavior, as well as of growth patterns which provide local detail were compared. Figure 10 shows four different pressure-saturation curves conducted at different pressure decline rates. A good agreement between experiments and simulations is noted. Some discrepancy exists at the later stages of the process

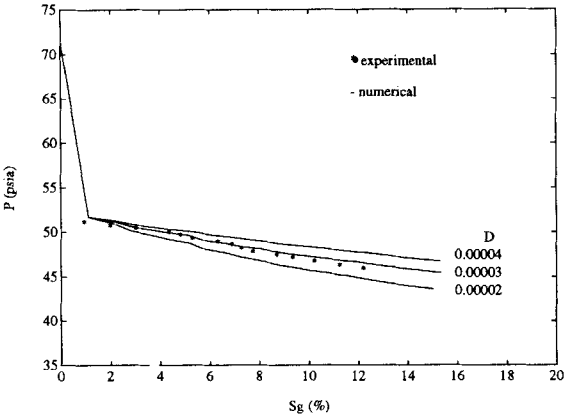

(a) Pressure-saturation curves at different values of D.

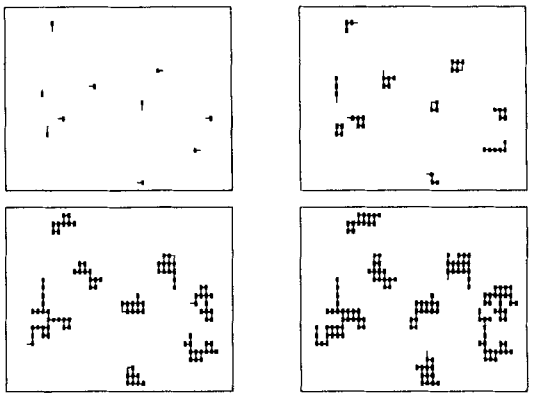

(b) Simulated gas cluster pattern

Figure 9. Pore network simulation of experimental results: $a = 1.44$ psi/h (9.92 kPa/h).

for $a = 8.16$ psi/h (56.2 kPa/h), where the numerical results tend to underestimate the saturations. This discrepancy is due to finite-size effects and to the lack of complete knowledge of the micromodel geometry. It should be pointed out that there is no reason to expect an asymptotic state at larger S_g, as some

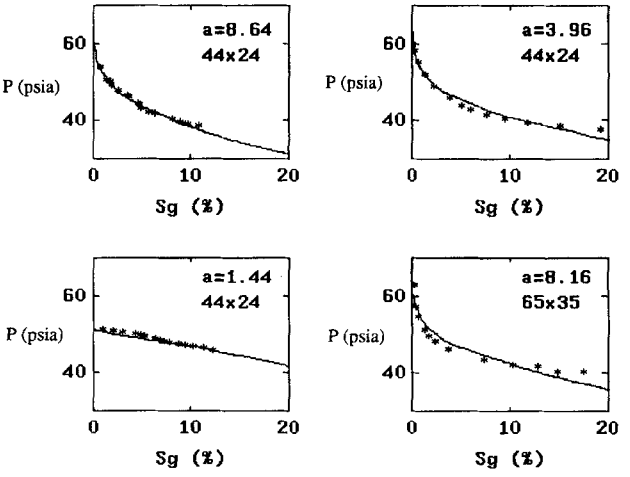

Figure 10. Experimental vs. pore network simulated P-Sg curves.

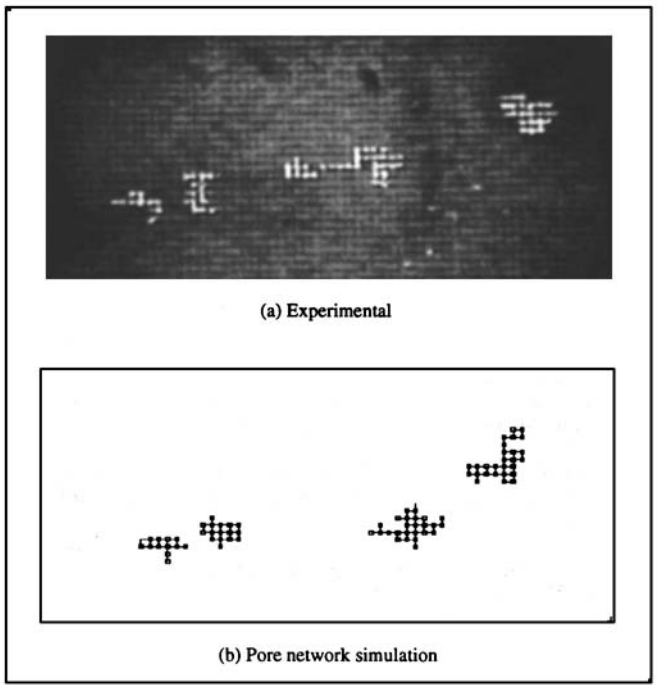

Figure 11. Comparison of local cluster growth patterns for $a = 5.24$ psi/h (36.1 kPa/h).

of the experiments in Figure 10 seem to indicate. Given the simplified nature of the numerical model, the uncertainty in the actual geometry of the pattern, and the fact that no *adjustable* parameters were used, the agreement between numerical simulations and experiments is quite acceptable. We should point out that a different number of nucleation sites were activated during these processes. In fact, because of the lack of reproducibility in the nucleation process for the reasons previously cited, the frequency of nucleation did not follow the expected trend of increasing with increases in a for permanently fixed sites. For example, an activation of 5, 7, 10 and 5 sites was observed in the experiments with pressure decline rates equal to 8.64, 3.96, 1.44 and 8.16 psi/h (59.5, 28.3, 9.9 and 56.2 kPa/h), respectively. As a result, definitive conclusions about the effect of a are not possible from these experiments, where nucleation is not reproducible. For fixed nucleation sites activated at different supersaturations, however, a sensitivity study using the numerical simulator and a theoretical analysis (Li and Yortsos, 1995) show that the effect of a is to lead to lower gas saturation for the same pressure at higher values of a as expected (which is also consistent with Figure 8).

A more stringent test of the simulator is to compare local growth patterns. Figure 11 shows the comparison between the experimental and numerical patterns for one of the experiments. The two patterns share many similar characteristics, although the patterns are not identical. To some extent, this is to be anticipated in view of the incomplete knowledge of the geometrical structure of the micromodel. Indeed, it is uncertain whether the capillary characteristics of the micromodel and the numerical model are identical. This produces different occupancy sequences, and therefore different growth patterns, in the two models. For the same reasons, a precise agreement between experimental and simulated patterns has not been obtained to our knowledge even in simpler external displacements, such as drainage. This uncertainty precludes the simulator from accurately matching the microscopic details in the more complex process of bubble growth. On the other hand, the experimentally observed "one-throat-at-a-time" growth mode was exactly matched during the simulation, indicating that the dominant mechanism was correctly simulated. These simulations have revealed that although the overall patterns are not in the global percolation regime, individual clusters still obey *local percolation* rules. Overall, the good agreement in matching the overall behavior is encouraging of the ability of the simulator to match important aspects of phase growth. The companion articles (Satik et al., 1995; Li and Yortsos, 1995) show how the simulator was used in the development of some simple theories and statistical models for bubble growth in the delineation of patterns and rates of growth, and in assessing the effect of nucleation. In particular, the important issues of the critical gas saturation and pressure decline rate are systematically investigated.

Conclusions

In this article, we conducted visualization experiments of bubble growth in glass micromodels taken to represent model porous media. The experiments confirmed many of the premises taken previously (Yortsos and Parlar, 1989), namely the onset of nucleation from different sites, the growth of vapor clusters in a ramified, rather than a compact, fashion, and the relevance of capillary effects to the growth process. The latter dictate a two-step growth mechanism, which at low and moderate pressure decline rates, occurs "one-throat-at a time." These experimental observations were subsequently incorporated into a pore network model, which includes nucleation, growth by mass transfer, and viscous and capillary effects. Numerical simulation of the experiments showed a good agreement in the overall features, but a poorer agreement in the microscale details. We attributed the latter to the uncertainty in the precise structure of the micromodel. The results were also consistent with simpler analytical results in the limit of slow growth. In the latter case, the relevance of a percolation approach to describe the growth process was verified. At the decline rates studied, local percolation rules also dictate the growth of each individual cluster. However, when many nucleation clusters are involved, their competition for solute results into a pore occupancy sequence different from global percolation as described in the companion articles (Satik et al., 1995; Li and Yortsos, 1995).

Notation

a = pressure decline rate
A = diffusion area
C = concentration of solute (dissolved gas)
D = diffusion coefficient
m = mass of gas phase
M_w = molecular weight
n = mole fraction of gas phase
Q = liquid withdrawal rate
R = ideal gas constant
S_{gc} = critical gas saturation
T = temperature

Greek letters

α = dimensionless solubility constant
μ = viscosity

Superscripts

f = flow
m = mass transfer

Acknowledgments

This article is a revised version of paper SPE 22589 presented at the SPE Annual Meeting, Dallas, TX, Oct. 6-9, 1991. This work was partly supported by a grant from Chevron Oil Field Research (now Chevron Petroleum Technology Corp.). Additional support was provided by the USC Center for the Study of Fractured Reservoirs, supported by Aramco, Mineral Management Services, State Lands Commission of California, Texaco E&P, and Unocal Science and Technology. All these sources of support are gratefully acknowledged. Useful discussions with Jairam Kamath are also acknowledged.

Literature Cited

Atchley, A. A., and A. Prosperetti, "The Crevice Model of Bubble Nucleation," *J. Acoust. Soc. Am.*, **86**(3), 1065 (1989).

Blunt, M., and P. King, "Relative Permeabilities from Two- and Three-Dimensional Pore-Scale Network Modeling," *Transport in Porous Media*, **6**, 407 (1991).

Chatzis, I., "Photofabrication Technique of 2-D Glass Micromodels," PRRC Report No. 82-12, New Mexico Institute of Technology (1982).

De Swaan, A., "Development of the Critical Gas Saturation," *J. Pet. Tech.*, 907 (1981).

Danesh, A., J. M. Peden, D. Krinis, and G. D. Henderson, "Pore Level Visual Investigation of Oil Recovery by Solution Gas Drive and Gas Injection," SPE 16956, SPE Meeting, Dallas (Sept. 27-30, 1987).

Doughty, C., and K. Pruess, "A Semianalytical Solution for Heat-Pipe Effects near High-Level Nuclear Waste Packages Buried in Partially Saturated Geological Media," *Int. J. Heat Mass Transf.*, **31**, 79 (1988).

Firoozabadi, A., B. Ottesen, and M. Mikklesen, "Measurement and Modeling of Supersaturation and Critical Gas Saturation: 1. Measurements," SPE 19694, SPE Meeting, San Antonio, TX (Oct. 8-11, 1989).

Homsy, G. M., "Viscous Fingering in Porous Media," *Ann. Rev. Fluid Mech.*, **19**, 271 (1987).

Hunt, E. B., Jr., and V. J. Berry, Jr., "Evolution of Gas from Liquids Flowing through Porous Media," *AIChE J.*, **2**, 560 (Dec., 1956).

Kamath, J., and R. E. Boyer, "Critical Gas Saturation and Supersaturation in Low Permeability Rocks," Paper SPE 26663, SPE Meeting, Houston (Oct. 3-6, 1993).

Kashchiev, D., and A. Firoozabadi, "Kinetics of the Initial Stage of Isothermal Gas Phase Formation," *J. Chem. Phys.*, **98**(6), 1 (1993a).

Kashchiev, D., and A. Firoozabadi, "Pressure and Volume Evolution during Gas Phase Formation in Solution Gas Drive Process," SPE 26286, preprint (1993b).

Kennedy, H. T., and C. R. Olson, "Bubble Formation in Supersaturated Hydrocarbon Mixtures," *AIME Trans.*, **195**, 271 (1952).

Kortekaas, T. F. M., and F. V. Poelgeest, "Liberation of Solution Gas during Pressure Depletion of Virgin and Watered-Out Reservoirs," SPE 19693, SPE Meeting, San Antonio, TX (Oct. 8-11, 1989).

Lenormand, R., E. Touboul, and C. Zarcone, "Numerical Models and Experiments on Immiscible Displacements in Porous Media," *J. Fluid Mech.*, **189**, 165 (1988).

Li, X., "Bubble Growth during Pressure Depletion in Porous Media," PhD Diss., Univ. of Southern California (May, 1993).

Li, X., and Y. C. Yortsos, "Critical Gas Saturation: Modeling and Sensitivity Study," SPE 26662, SPE Meeting, Houston (Oct. 6-9, 1993).

Li, X., and Y. C. Yortsos, "Bubble Growth and Stability in an Effective Porous Medium," *Phys. Fluids A*, **6**, 1663 (1994).

Li, X., and Y. C. Yortsos, "Theory of Multiple Bubble Growth in Porous Media by Solute Diffusion," *Chem. Eng. Sci.*, in press (1995).

Lifshitz, I. M., and V. V. Slyozov, "The Kinetics of Precipitation from Supersaturated Solid Solutions," *J. Phys. Chem. Solids*, **19**, 35 (1961).

Moulu, J. C., and D. Longeron, "Solution-Gas Drive: Experiments and Simulation," Euro. Symp. on Improved Oil Recovery, Budapest, Hungary (Apr., 1989).

Payatakes, A. C., and M. M. Dias, "Immiscible Microdisplacement and Ganglion Dynamics in Porous Media," *Rev. in Chem. Eng.*, **2**, 85 (1984).

Plesset, M. S., and A. Prosperetti, "Bubble Dynamics and Cavitation," *Ann. Rev. Fluid Mech.*, **9**, 145 (1977).

Quinn, E. L., and C. L. Jones, *Carbon Dioxide*, Reinhold, New York (1936).

Rothman, D. H., "Cellular-Automaton Fluids: A Model for Flow in Porous Media," *Geophys.*, **53**, 509 (1988).

Satik, C., "Studies in Vapor-Liquid Flow in Porous Media," PhD Diss., Univ. of Southern California (May, 1994).

Satik, C., X. Li, and Y. C. Yortsos, "Scaling of Bubble Growth in a Porous Medium," *Phys. Rev. E.*, in press (1995).

Schubert, G., and J. M. Straus, "Two-Phase Convection in a Porous Medium," *J. Geophys. Res.*, **82**, 3411 (1977).

Scriven, L. E., "On the Dynamics of Phase Growth," *Chem. Eng. Sci.*, **10**, 1 (1959).

Stewart, C. R., F. F. Craig, and R. A. Morse, "Determination of Limestone Performance Characteristics by Model Flow Tests," *AIME Trans.*, **198**, 93 (1953).

Thome, J. R., *Enhanced Boiling Heat Transfer*, Hemisphere, New York (1990).

Vivian, J. E., and C. J. King, "Diffusivities of Slightly Soluble Gases in Water," *AIChE J.*, **10**, 220 (1964).

Wieland, D. R., and H. T. Kennedy, "Measurement of Bubble Frequency in Cores," *AIME Trans.*, **210**, 123 (1957).

Yortsos, Y. C., and M. Parlar, "Phase Change in Binary Systems in Porous Media: Application to Solution Gas Drive," SPE 19697, SPE Meeting, San Antonio, TX (Oct. 8-11, 1989).

Yousfi, El., C. Zarcone, S. Bories, and R. Lenormand, "Liberation of Solution Gas during Pressure Depletion in a 2-Dimensional Porous Medium," IFP Research Conf., Arles, France (May 14-18, 1990).

Yousfi, El., C. Zarcone, S. Bories, and R. Lenormand, "Mechanisms of Solution Gas Liberation during Pressure Depletion in Porous Media," *C. R. Acad. Sci. Paris, t.*, **313**, Ser. II, 1093 (1991).

Manuscript received Nov. 12, 1993, and revision received Feb. 25, 1994.